Orbital Angular Momentum Induced Spin Polarization of 2D Metallic Bands

Takahiro Kobayashi,[1,*] Yoshitaka Nakata,[2] Koichiro Yaji,[3] Tatsuya Shishidou,[4] Daniel Agterberg,[4] Shunsuke Yoshizawa,[3] Fumio Komori,[5] Shik Shin,[5] Michael Weinert,[4] Takashi Uchihashi,[6] and Kazuyuki Sakamoto[7,†]

[1]*Department of Material and Life Science, Osaka University, Osaka 565-0871, Japan*
[2]*Department of Materials Science, Chiba University, Chiba 263-8522, Japan*
[3]*Research Center for Advanced Measurement and Characterization, National Institute for Materials Science, Ibaraki 305-0047, Japan*
[4]*Department of Physics, University of Wisconsin-Milwaukee, Wisconsin 53201, USA*
[5]*Institute for Solid State Physics, The University of Tokyo, Chiba 277-8581, Japan*
[6]*International Center for Materials Nanoarchitectonics (WPI-MANA), National Institute for Materials Science, Ibaraki 305-0044, Japan*
[7]*Department of Applied Physics, Osaka University, Osaka 565-0871, Japan*

(Received 25 June 2020; revised 12 August 2020; accepted 23 September 2020; published 19 October 2020)

The electrons in 2D systems with broken inversion symmetry are spin-polarized due to spin-orbit coupling and provide perfect targets for observing exotic spin-related fundamental phenomena. We observe a Fermi surface with a novel spin texture in the 2D metallic system formed by indium double layers on Si (111) and find that the primary origin of the spin-polarized electronic states of this system is the orbital angular momentum and not the so-called Rashba effect. The present results deepen the understanding of the physics arising from spin-orbit coupling in atomic-layered materials with consequences for spintronic devices and the physics of the superconducting state.

DOI: 10.1103/PhysRevLett.125.176401

The combination of spin-orbit coupling (SOC) with broken spatial inversion symmetry leads to a variety of exotic spin-related fundamental phenomena [1] that are of interest both for fundamental science—e.g., creation of novel superconducting states [2]—and for applications, since they contain key concepts needed to realize future semiconductor spintronics devices [3–5]. The spin-polarized electronic bands in two-dimensional (2D) atomic layers formed on solid surfaces is one such phenomenon. The so-called Rashba-Bychkov (or simply Rashba) effect [6] provides the basic model for this phenomenon: the spin-polarized 2D electronic states arise from the gradient of the potential or, more precisely, from the asymmetric charge distribution along the direction normal to the 2D layer [7,8].

In the case of an ideal 2D electron gas, the Rashba effect produces a pair of spin-polarized bands in $\mathbf{k}$ space with the spin oriented perpendicular to both the surface normal and momentum directions (Fig. S1 of the Supplemental Material [9]). This ideal Rashba-type spin splitting was observed in the L gap of Au(111) over 20 years ago [13–15] and in the L gap of Ag(111) and Cu(111) more recently [16]. In contrast to these results on noble metals, sizable Rashba-type spin splittings [17,18] and spin textures that differ from the ideal Rashba effect [19–26] have been reported for 2D atomic layers formed on solid surfaces. Peculiar spin textures have also been observed in noncentrosymmetric bulk materials [27–29]. Chiral orbital angular momentum (OAM) has been reported to play a role in the size of the spin splitting [18,30,31], and deviations in spin texture from the ideal case have been attributed to the perturbation induced by the symmetry of the atomic structure and/or from the entanglement of spin and orbital momenta; i.e., the spin-polarized bands are still explained in the framework of the Rashba effect in these studies. (In this Letter, we use "chiral OAM" as an effect that produces spin texture similar to that of the Rashba effect.) A fundamental understanding of the spin physics arising from the SOC in atomic layer materials is necessary for the realization of novel spintronics devices and possible topological or novel superconductors formed by 2D materials with spin-polarized states [2,32,33].

In this Letter, we report that the spin texture of the Fermi surface (FS) of a Si(111) surface covered with two layers of indium (In) can be explained by the OAM alone, i.e., without invoking the Rashba effect. The atomic structure of the In double layer on Si(111) is shown in Figs. 1(a) and 1(b). As shown in the figure, an adsorbed bilayer of In, which forms a square lattice on the triangular Si lattice, gives rise to a $(\sqrt{7} \times \sqrt{3})$ reconstructed structure [which we denote simply as $(\sqrt{7} \times \sqrt{3})$-In]. This $(\sqrt{7} \times \sqrt{3})$-In, which has a mirror plane along the $[11\bar{2}]$ direction and thus has a C_{1h} symmetry, is known to have metallic surface states [10,34] and to become superconducting below 3 K [35,36]. So far, however, spin-polarized FSs have not been observed experimentally, nor discussed theoretically for this system, although a spin splitting of the FS affects the interpretation of the superconductivity. By using an experimental setup with both high energy and momentum resolution, we succeed in observing

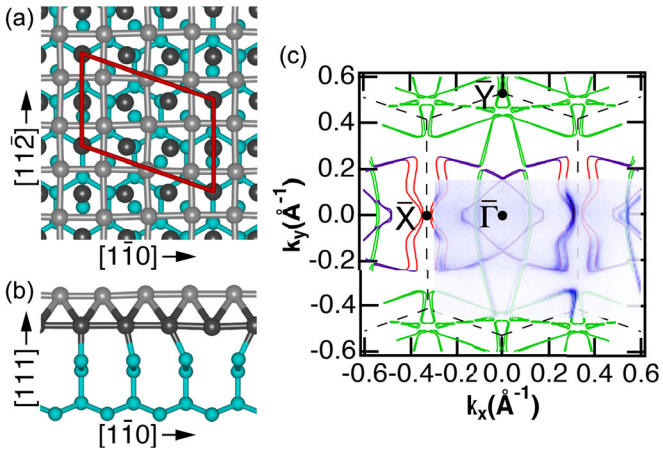

FIG. 1. (a) Top view and (b) side view of $(\sqrt{7}\times\sqrt{3})$-In. The red solid line in (a) represents the unit cell. Green circles in (a) and (b) represent Si atoms, light gray circles represent first layer In atoms, and dark gray circles represent In of the second layer. (c) The FS of $(\sqrt{7}\times\sqrt{3})$-In. The theoretical calculation (green, red, and purple solid lines) is overlaid by the experimental data (blue). The Brillouin zone is indicated by black broken lines. $\bar{\Gamma}-\bar{Y}$ corresponds to the [11$\bar{2}$] direction and $\bar{X}-\bar{\Gamma}$ to the [1$\bar{1}$0] direction.

the spin-polarized FS of $(\sqrt{7}\times\sqrt{3})$-In. The origin of this spin-polarized FS is established both experimentally, by high-resolution angle-resolved photoelectron spectroscopy (ARPES) and spin and angle-resolved photoelectron spectroscopy (SARPES), and theoretically by density-functional theory (DFT). Our results demonstrate that this system is a candidate as a few atomic layer superconductor that develops a spatially modulated, or pair density wave order, under in-plane magnetic fields.

The details of high-resolution ARPES and SARPES measurements as well as the DFT calculations performed in the present study are described in the Supplemental Material [9]. $(\sqrt{7}\times\sqrt{3})$-In was prepared by depositing approximately three monolayers of In onto a clean Si(111) surface at 300 K, followed by annealing at 600 K for a couple minutes. The sample quality was confirmed by the observations of sharp spots with low background intensity in low-energy electron diffraction (see Fig. S2 in Supplemental Material [9]) and sharp surface states in ARPES spectra.

The experimentally obtained FS of $(\sqrt{7}\times\sqrt{3})$-In is shown in Fig. 1(c) together with the FS obtained theoretically including the SOC. The experimental FS, which is obtained from the summation of the photoelectron intensity within a 5 meV energy window from the Fermi level, shows good agreement with that reported in a previous study [34], but with clear splittings. Since the theoretical FS obtained without including the SOC does not have these splittings, as shown in [10] and also in Fig. 3(b), those observed in the present study result from SOC. In Ref. [34], this complex looking FS is attributed to the backfolding of two metallic bands in the reduced Brillouin zone; i.e., a two-dimensional nearly-free-electron metallic band forms a circular FS and a metallic band forming a small FS around the $\bar{X}$, with most of the FS formed by the former band. To simplify the discussion, we hereafter call the FS indicated by the green lines in Fig. 1(c) the "circular FS" and that indicated by the red and purple lines as the "side-part butterfly FS" and "cross-part butterfly FS," respectively. The largest splitting of the butterfly FS was 0.035 Å^{-1} and that of the circular one was 0.007 Å^{-1}. Since ARPES measurements with lower energy and momentum resolution will merge the split FSs into one, the difference in the splitting could be one of the reasons for the difference in the linewidths of the butterfly and circular FSs in the previous study [34], where the butterfly FS is much broader than the circular one.

The SARPES measurements reveal the spin vectors of both the circular and the butterfly FSs. As shown in the spin-resolved energy distribution curves of Fig. 2(a), the y component mainly contributes to the spin vectors at the point A of the circular FS with a small contribution from the x component, implying that the spin vectors are tangential to the FS as expected for ideal Rashba spins. On the other hand, the spin-resolved momentum distribution curves in Figs. 2(b),2(d), and 2(e) show that the main component of the spin vectors for cuts B, D, and E of the butterfly FS is the x component, which cannot be explained by either the Rashba effect or the chiral OAM. At the cut C, which is slightly off of $k_y=0$ and where the two split FSs almost touch each other, the small splitting in k_x can be seen in the x and y components but barely in the z component. Furthermore, the sign of the x component flips when k_y changes sign: the spins of the inner and outer butterfly are oppositely directed, along $-k_x$ and $+k_x$, respectively, for $k_y<0$ as clearly seen in Figs. 2(e) and S3(c) [9] and flip for $k_y>0$, cf. Figs. 2(e) and 2(b). Extracting the spin directions from other spectra is complicated by final state effects [9], which can affect the intensities for the low photon energies used here. However, assuming the original intensities of the two spin directions to be similar, the peak positions provide a rough estimate of the spin directions, as shown in Fig. 2(f). This simple procedure is supported by the agreement with the theoretically obtained spin polarization shown in Fig. 3(a). The spin flip at $k_y=0$ results from the C_{1h} symmetry with a mirror plane on the $\bar{\Gamma}-\bar{Y}$ line of the system. In particular, the spin-orbit coupling takes the form $\vec{g}(\vec{k})\cdot\vec{S}(\vec{k})$, where $\vec{S}(\vec{k})$ is the spin at momentum $\vec{k}$ and $\vec{g}(\vec{k})$ characterizes the spin-orbit coupling that satisfies $\vec{g}(\vec{k})=-\vec{g}(-\vec{k})$ due to time-reversal symmetry. The mirror symmetry implies that $g_x(k_x,k_y)=-g_x(k_x,-k_y)$, yielding the aforementioned spin flip [9]. This mirror symmetry also implies $g_y(k_x,k_y)=g_y(k_x,-k_y)$ and $g_z(k_x,k_y)=g_z(k_x,-k_y)$.

The observed spin texture of the butterfly FS immediately rules out both the Dresselhaus effect [37] and a Zeeman field as the origin for the spin parallel to the wave

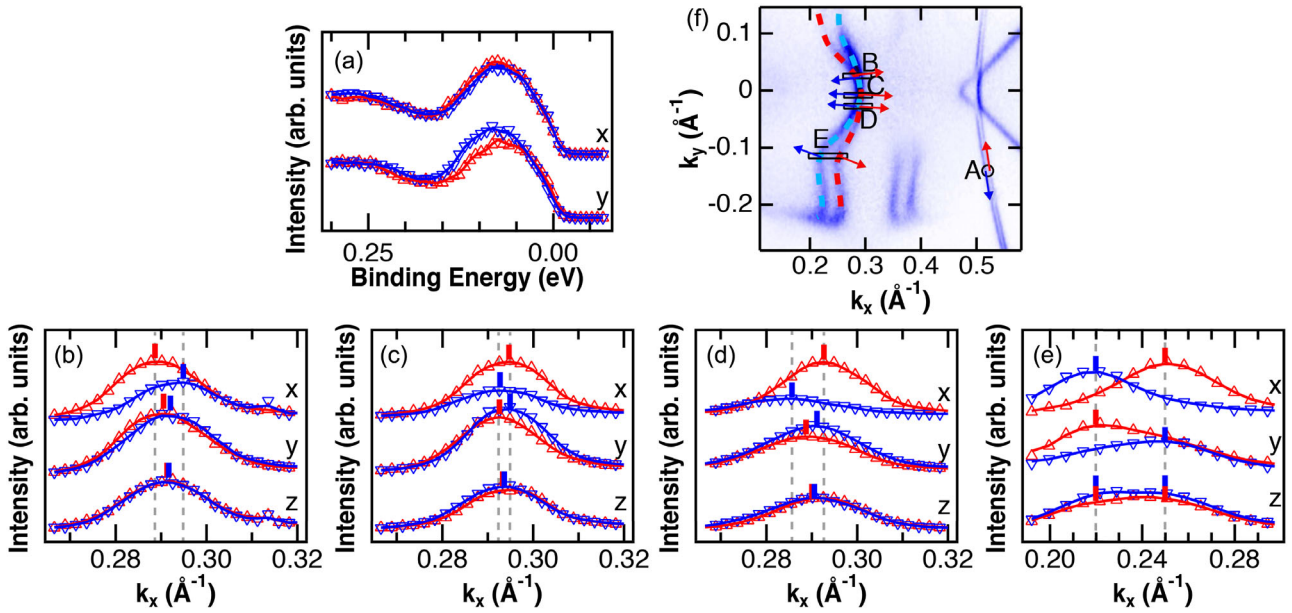

FIG. 2. (a) Spin-resolved energy distribution curves measured at point A in the FS shown in (f). (b)–(e) Spin-resolved momentum distribution curves measured at the cuts B, C, D, and E points. The x, y, and z axes correspond to the $[1\bar{1}0]$, $[11\bar{2}]$, and $[111]$ directions of the substrate, respectively. Red data indicate spins in the positive direction of each axis, and blue data are spins in the negative direction of each axis. The red and blue bars indicate the peak position in each spectrum and the gray dashed lines in (b)–(e) are the k_x value of the FS obtained by SARPES. Error bars are smaller than the symbol sizes and not shown. The directions of the spin estimated from the results in (a)–(e) are schematically represented in the experimental FS in (f).

vector (see Fig. S1 of the Supplemental Material [9]). To understand where this spin texture originates from, we have examined the OAM induced in the In $5p$ shell when no SOC is included [38]. The directions of the OAM on the FS [Fig. 3(b)] and the spin vectors of the inner circular and inner butterfly FSs [Fig. 3(a)] show good correspondence, and the OAM coincides with the spin vector as shown in Fig. S4 of the Supplemental Material [9], where the inner product of the OAM and spin vectors shows values between 0.98 and 1.0. Figures 3(c)–3(e) display the electron probability isosurface at the k point on the circular FS indicated by the open circle in Fig. 3(b) in the xy, xz, and yz planes, and Figs. 3(f)–3(h) for the k point on the side-part butterfly FS indicated by the open square in Fig. 3(b). For the circular FS, as shown in Figs. 3(d) and 3(e), those located in the first In layer move circularly in the xz plane around the nuclei and produce sizable OAM along the y axis. For the side-part butterfly FS, on the other hand, the electrons located in the second In layer tend to have rotating state in the yz plane as shown in Fig. 3(h). (More interaction with Si substrate is noticed here than in the case of circular FS.) A detailed wave function analysis in terms of atomic orbital is given in the Supplemental Material [9] for the three particular k points marked in Fig. 3(b). When the SOC is turned on, the effective magnetic field that is perpendicular to the plane of electron's circular motion lifts the spin degeneracy and consequently orients the spin vectors in the $\pm y(\pm x)$ direction for the k point indicated by the open circle (square).

The spin vectors at the cross-part butterfly FS are not Rashba-like spins, although that is the origin previously ascribed [34]. In fact, as shown in Figs. 3(i)–3(k), the electrons at the k point indicated by the open triangle in Fig. 3(b) bear more resemblances to those in the side-part butterfly FS than to the circular FS; there exists a considerable amount of interaction with the interface Si state, and the individual In atoms show highly inhomogeneous contributions to the electron map both in the first and second In layers. This means that the cross-part butterfly FS should have the same origin as that of the side-part butterfly FS. Regarding the splitting in k, it hardly changes on the circular FS. On the other hand, the splitting at the cross-part butterfly FS is much smaller than that at the side part, and the size of the spin splitting is almost proportional to the OAM size, which is demonstrated by the length of the arrows in Fig. 3(b). The OAM size and the spin splitting are 0.015 and 17 meV, and 0.058 and 87 meV, at the k points marked by a triangle and a square on the butterfly FS. This behavior indicates that the effect of SOC is dominantly the band diagonal first-order effect.

The OAM size at the k point marked by a circle is 0.06, a value that is very close to that of the point marked by a square on the butterfly FS, though the split in k differs significantly at these two points. This difference is due to fact that SOC induces spin split along the energy direction, and the split along k is a result of this energy split; i.e., the splitting in k depends on the gradient of the band dispersion, and in the present case the steep dispersion

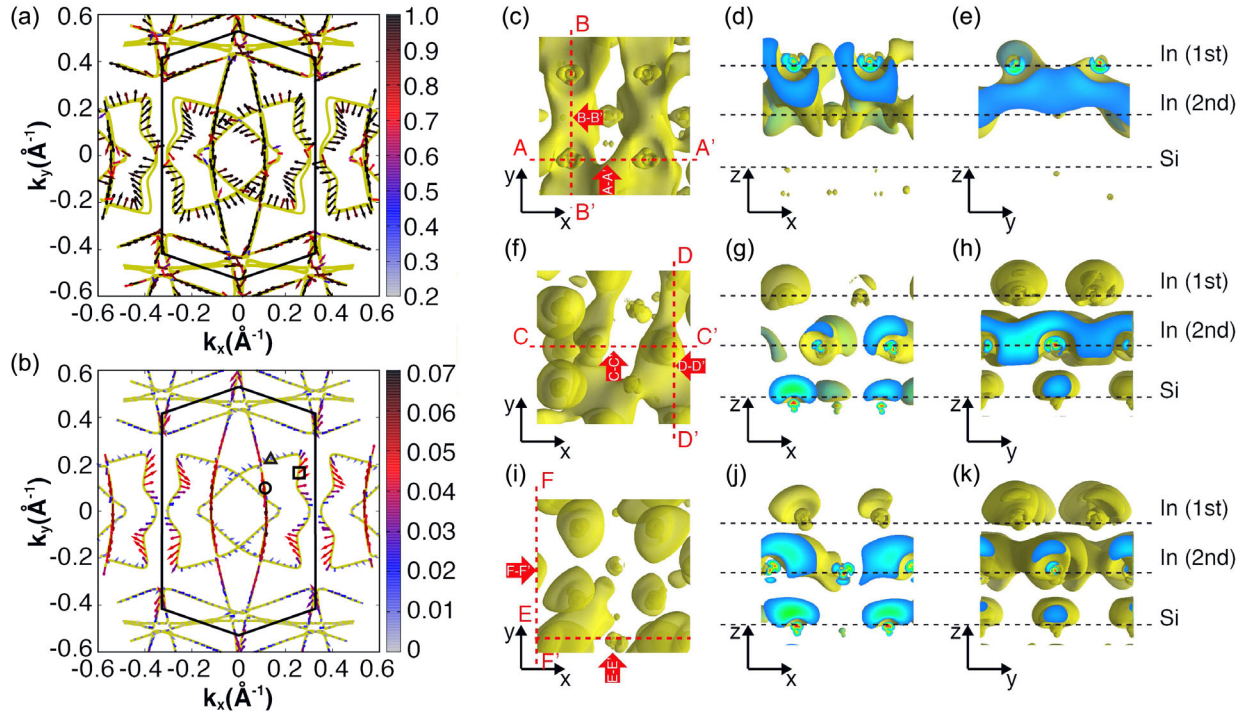

FIG. 3. (a) Theoretically obtained spin polarization (arrows) of the FS (inner side only). (b) Theoretical OAM distribution (arrows) in absence of SOC. (c)–(k) Real space electron probability isosurfaces (0.008 Å^{-3}) corresponding to selected k points on the FS. Isosurfaces (c)–(e), (f)–(h), and (i)–(k) correspond, respectively, to the k points marked by a circle, square, and triangle in (b). (d) [(g), (j)] is the cross sectional view of $A - A'$ ($C - C'$, $E - E'$) seen from direction of the arrow marked with the same labeling in (c), and (e) [(h), (k)] is that of $B - B'$ ($D - D'$, $F - F'$). In (d), (e), (g), (h), (j), and (k), the blue areas are the cross sections at the plane and the yellow ones are the isosurfaces behind the planes.

of the circular FS leads to a k splitting smaller than that at the k point marked by a square as shown in Fig. 4. (The gradients are ~2.8 eV Å in 4(a), 14.7 eV Å in 4(b), and the OAM size and spin splitting at other k points are shown in Fig. S4 of the Supplemental Material [9].) These results demonstrate that the primary origin of the spin-polarized states of $(\sqrt{7} \times \sqrt{3})$-In is OAM and not the Rashba effect.

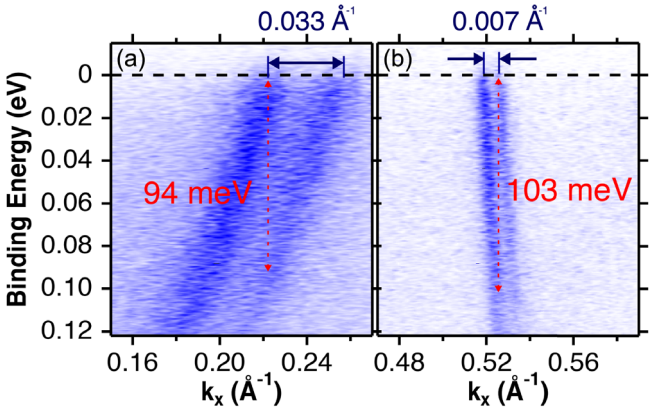

FIG. 4. Band dispersions (ARPES intensity map) of (a) the butterfly FS at $k_y = -0.15$ Å^{-1} close to the point marked by a square in Fig. 3(b), and (b) the circular FS at $k_y = -0.1$ Å^{-1}.

It is interesting to examine the role of the observed SOC on the superconducting state. In particular, the strength of this coupling (on the order of 0.1 eV) is much larger than the superconducting gap (with a transition temperature of 3 K [35,36]), implying that it can significantly affect the superconducting state. One possible consequence is a topological superconducting state which can arise if odd-parity pairing interactions are strong enough [39]. While this is possible, it is more likely that the superconducting state is a usual s-wave pairing state. Even in this case, the SOC has nontrivial consequences, particularly in the presence of an applied in-plane Zeeman field. First, the critical field can surpass the Pauli limiting field, as the following expression reveals:

$$\ln\left(\frac{T_c(h)}{T_c}\right) = 2\left\langle f\left(\frac{\vec{g}(\vec{k})\cdot\vec{h}}{\pi T_c|\vec{g}(\vec{k})|}\right)\right\rangle_k, \qquad (1)$$

where $T_c(h)$ is the transition temperature in a Zeeman field H ($h = \mu_B H$) and the subscript k means to take an average over the FS. In this expression,

$$f(x) = \mathrm{Re}\sum_{n=1}^{\infty}\left(\frac{1}{2n-1+ix} - \frac{1}{2n-1}\right), \qquad (2)$$

which captures the suppression of T_c with applied field (in the usual Pauli limiting case, the variable $x = h/\pi T_c$ that is always larger than in the above equation). Since the FS average of OAM field of Fig. 3(b) gives $\langle \hat{g}_\alpha^2 \rangle_k = 0.51, 0.45,$ and 0.03 for $\alpha = x, y, z$, respectively, this implies that the Pauli critical field enhancement is expected to be large for the c axis (indicating that the critical field is only orbitally limited) and to be moderate for in-plane fields. Second, the combination of broken inversion symmetry and broken time-reversal symmetry in the presence of an in-plane Zeeman field must lead to a spatial varying, pair density wave order [40], in which the gap takes the form $\Delta(x, y) = \Delta_0 e^{i(q_x x + q_y y)}$, where $q_x \neq 0$ and $q_y = 0$ for a Zeeman field applied along the y axis ($q_x = 0$ and $q_y \neq 0$ for a field applied along the x axis). Such a state can give rise to fractional vortices if an additional field is applied along the z axis [2,40] and is closely related to novel magnetoelectric effects [41].

Based on the above results, we conclude that OAM induces various spin textures, ranging from the Rashba-type to a type that cannot be explained based on the Rashba effect, but which depends on the distribution of the electron density. In the present case, the electron probability density located on the first layer atoms produces a circular FS with Rashba-type spin texture, while that located on the second layer In atoms forms butterfly FSs with the spin mostly parallel to the wave vectors. Extension of the present model of OAM induced spin-polarized bands to other 2D atomic layers materials and the possibility of producing a pair density wave superconductor using $(\sqrt{7} \times \sqrt{3})$-In are exciting directions for future work.

The authors thanks P. Krüger of Chiba University Japan for fruitful discussion. This research is supported by the JSPS Grant-in-Aid for Scientific Research (B) 19H02592, and the JSPS Grant-in-Aid for Scientific Research on Innovative Areas 3D Active-Site Science 17H05211 and Nano-Material Optical-Manipulation 17H05461, the World Premier International Research Center (WPI) Initiative on Materials Nanoarchitectonics, MEXT, Japan, and by the National Science Foundation, Grant No. EFMA-1741673.

*tkobayashi@ap.eng.osaka-u.ac.jp
†kazuyuki_sakamoto@ap.eng.osaka-u.ac.jp

[1] S. Murakami, New J. Phys. **9**, 356 (2007).
[2] M. Smidman, M. B. Salamon, H. Q. Yuan, and D. F. Agterberg, Rep Prog. Phys. **80**, 036501 (2017).
[3] S. Datta and B. Das, Appl. Phys. Lett. **56**, 665 (1990).
[4] S. A. Wolf, D. D. Awschalom, R. A. Buhrman, J. M. Daughton, S. von Molnár, M. L. Roukes, A. Y. Chtchelkanove, and D. M. Treger, Science **294**, 1488 (2001).
[5] D. D. Awschalom and M. E. Flatté, Nat. Phys. **3**, 153 (2007).
[6] Y. A. Bychkov and E. I. Rashba, JETP Lett. **39**, 78 (1984), http://www.jetpletters.ac.ru/ps/1264/article_19121.shtml.
[7] M. Nagano, A. Kodama, T. Shishidou, and T. Oguchi, J. Phys. Condens. Matter **21**, 064239 (2009).
[8] K. Yaji, Y. Ohtsubo, S. Hatta, H. Okuyama, H. Miyamoto, T. Okuda, A. Kimura, H. Namatame, M. Taniguchi, and T. Aruga, Nat. Commun. **1**, 17 (2010).
[9] See Supplemental Material at http://link.aps.org/supplemental/10.1103/PhysRevLett.125.176401 for details of the methods, model spin textures, momentum distribution curves of the butterfly FS, correlation of OAM and spin, orbital analysis, and symmetry induced spin flip, which includes Refs. [10–12].
[10] K. Uchida and A. Oshiyama, Phys. Rev. B **87**, 165433 (2013).
[11] K. Yaji, A. Harasawa, K. Kuroda, S. Toyohisa, M. Nakayama, Y. Ishida, A. Fukushima, S. Watanabe, C.-T. Chen, F. Komori, and S. Shin, Rev. Sci. Instrum. **87**, 053111 (2016).
[12] M. Weinert, G. Schneider, R. Podloucky, and J. Redinger, J. Phys. Condens. Matter. **21**, 084201 (2009).
[13] S. LaShell, B. A. McDougall, and E. Jensen, Phys. Rev. Lett. **77**, 3419 (1996).
[14] G. Nicolay, F. Reinert, S. Hüfner, and P. Blaha, Phys. Rev. B **65**, 033407 (2001).
[15] M. Hoesch, M. Muntwiler, V. N. Petrov, M. Hengsberger, L. Patthey, M. Shi, M. Falub, T. Greber, and J. Osterwalder, Phys. Rev. B **69**, 241401(R) (2004).
[16] K. Yaji, A. Harasawa, K. Kuroda, R. Li, B. Yan, F. Komori, and S. Shin, Phys. Rev. B **98**, 041404(R) (2018).
[17] C. R. Ast, J. Henk, A. Ernst, L. Moreschini, M. C. Falub, D. Pacilé, P. Bruno, K. Kern, and M. Grioni, Phys. Rev. Lett. **98**, 186807 (2007).
[18] M. Ünzelmann, H. Bentmann, P. Eck, T. Kißlinger, B. Geldiyev, J. Rieger, S. Moser, R. C. Vidal, K. Kißner, L. Hammer, M. A. Schneider, T. Fauster, G. Sangiovanni, D. Di Sante, and F. Reinert, Phys. Rev. Lett. **124**, 176401 (2020).
[19] K. Sakamoto, T. Oda, A. Kimura, K. Miyamoto, M. Tsujikawa, A. Imai, N. Ueno, H. Namatame, M. Taniguchi, P. E. J. Eriksson, and R. I. G. Uhrberg, Phys. Rev. Lett. **102**, 096805 (2009).
[20] P. Höpfner, J. Schäfer, A. Fleszar, J. H. Dil, B. Slomski, F. Meier, C. Loho, C. Blumenstein, L. Patthey, W. Hanke, and R. Claessen, Phys. Rev. Lett. **108**, 186801 (2012).
[21] Y. Ohtsubo, S. Hatta, H. Okuyama, and T. Aruga, J. Phys. Condens. Matter **24**, 092001 (2012).
[22] K. Nakajin and S. Murakami, Phys. Rev. B **91**, 245428 (2015).
[23] E. Annese *et al.*, Phys. Rev. Lett. **117**, 016803 (2016).
[24] C. Brand, S. Muff, M. Fanciulli, H. Pfnür, M. C. Tringides, J. H. Dil, and C. Tegenkamp, Phys. Rev. B **96**, 035432 (2017).
[25] R. Noguchi, K. Kuroda, K. Yaji, K. Kobayashi, M. Sakano, A. Harasawa, T. Kondo, F. Komori, and S. Shin, Phys. Rev. B **95**, 041111(R) (2017).
[26] K. Yaji, A. Visikovskiy, T. Iimori, K. Kuroda, S. Hayashi, T. Kajiwara, S. Tanaka, F. Komori, and S. Shin, Phys. Rev. Lett. **122**, 126403 (2019).
[27] R. Suzuki, M. Sakano, Y. J. Zhang, R. Akashi, D. Morikawa, A. Harasawa, K. Yaji, K. Kuroda, K. Miyamoto, T. Okuda, K. Ishizaka, R. Arita, and Y. Iwasa, Nat. Nanotechnol. **9**, 611 (2014).
[28] L. L. Tao and E. Y. Tsymbal, Nat. Commun. **9**, 2763 (2018).

[29] J. Krempaský, M. Fanciulli, L. Nicolaï, J. Minár, H. Volfová, O. Caha, V. V. Volobuev, J. Sánchez-Barriga, M. Gmitra, K. Yaji, K. Kuroda, S. Shin, F. Komori, G. Springholz, and J. H. Dil, Phys. Rev. Research **2**, 013107 (2020).
[30] S. R. Park, C. H. Kim, J. Yu, J. H. Han, and C. Kim, Phys. Rev. Lett. **107**, 156803 (2011).
[31] D. Go, J.-P. Hanke, P. M. Buhl, F. Freimuth, G. Bihlmayer, H.-W. Lee, Y. Mokrousov, and S. Blügel, Sci. Rep. **7**, 46742 (2017).
[32] J. D. Sau, R. M. Lutchyn, S. Tewari, and S. Das Sarma, Phys. Rev. Lett. **104**, 040502 (2010).
[33] C. Lei, H. Chen, and A. H. MacDonald, Phys. Rev. Lett. **121**, 227701 (2018).
[34] E. Rotenberg, H. Koh, K. Rossnagel, H. W. Yeom, J. Schäfer, B. Krenzer, M. P. Rocha, and S. D. Kevan, Phys. Rev. Lett. **91**, 246404 (2003).
[35] T. Zhang, P. Cheng, W.-J. Li, Y.-J. Sun, G. Wang, X.-G. Zhu, K. He, L. Wang, X. Ma, X. Chen, Y. Wang, Y. Liu, H.-Q. Lin, J.-F. Jia, and Q.-K. Xue, Nat. Phys. **6**, 104 (2010).
[36] T. Uchihashi, P. Mishra, M. Aono, and T. Nakayama, Phys. Rev. Lett. **107**, 207001 (2011).
[37] G. Dresselhaus, Phys. Rev. **100**, 580 (1955).
[38] S. Oh and H. J. Choi, Sci. Rep. **7**, 2024 (2017).
[39] A. P. Schnyder and S. Ryu, Phys. Rev. B **84**, 060504(R) (2011).
[40] D. F. Agtergerg, J. C. S. Davis, S. D. Edkins, E. Fradkin, D. J. Van Harlingen, S. A. Kivelson, P. A. Lee, L. Radzihovsky, J. M. Tranquada, and Y. Wang, Annu. Rev. Condens. Matter Phys. **11**, 231 (2020).
[41] Wen-Yu He and K. T. Law, Phys. Rev. Research **2**, 012073 (R) (2020).